applied optics

How daylight influences high-order chromatic descriptors in natural images

Juan Ojeda, Juan Luis Nieves,* and Javier Romero

Department of Optics, Sciences Faculty, University of Granada, Granada 18071, Spain
**Corresponding author: jnieves@ugr.es*

Received 10 February 2017; revised 28 April 2017; accepted 29 April 2017; posted 3 May 2017 (Doc. ID 286551); published 25 May 2017

Despite the global and local daylight changes naturally occurring in natural scenes, the human visual system usually adapts quite well to those changes, developing a stable color perception. Nevertheless, the influence of daylight in modeling natural image statistics is not fully understood and has received little attention. The aim of this work was to analyze the influence of daylight changes in different high-order chromatic descriptors (i.e., color volume, color gamut, and number of discernible colors) derived from 350 color images, which were rendered under 108 natural illuminants with Correlated Color Temperatures (CCT) from 2735 to 25,889 K. Results suggest that chromatic and luminance information is almost constant and does not depend on the CCT of the illuminant for values above 14,000 K. Nevertheless, differences between the red-green and blue-yellow image components were found below that CCT, with most of the statistical descriptors analyzed showing local extremes in the range 2950 K–6300 K. Uniform regions and areas of the images attracting observers' attention were also considered in this analysis and were characterized by their patchiness index and their saliency maps. Meanwhile, the results of the patchiness index do not show a clear dependence on CCT, and it is remarkable that a significant reduction in the number of discernible colors (58% on average) was found when the images were masked with their corresponding saliency maps. Our results suggest that chromatic diversity, as defined in terms of the discernible colors, can be strongly reduced when an observer scans a natural scene. These findings support the idea that a reduction in the number of discernible colors will guide visual saliency and attention. Whatever the modeling is mediating the neural representation of natural images, natural image statistics, it is clear that natural image statistics should take into account those local maxima and minima depending on the daylight illumination and the reduction of the number of discernible colors when salient regions are considered.

OCIS codes: (330.1690) Color; (330.1720) Color vision.

https://doi.org/10.1364/AO.56.00G120

1. INTRODUCTION

Natural image statistics have deserved a lot of attention during the last years supporting the idea that the Human Visual System (HVS) evolved to be adapted to the natural environment [1]. Different studies have characterized the properties of the natural images with the aim to understand our visual coding [2]. Important results in color vision encoding have been derived from the use of this strategy. The transformation of the cones' responses into opponent chromatic channels can be justified by the reduction of visual redundancy [3,4]. Also, color and space properties of receptive fields [5] and cortical cells [6] are from redundancy analysis and obtained, for instance, from independent components analysis.

The color signal of objects depends on the spectral reflectance of their surfaces and the spectral power distribution (SPD) of the light impinging on it. Global temporal variations in the SPD, as a result of the sun's location and weather conditions, have been characterized and expressed in terms of Correlated Color Temperature (CCT) [7]. However, more abrupt local variations of illumination may be included in natural images due to their complex spatial structures, including occlusions, mutual reflections, and shading [8]. Despite these global and local daylight changes naturally occurring in natural scenes, the HVS usually adapts quite well to those changes, developing a stable color perception [9].

The influence of daylight in modeling natural image statistics is not fully understood and has received little attention; only the chromatic diversity and color gamut expanded under different daylights have been analyzed by some authors. Martinez-Verdú *et al.* [10] established the variations of the number of colors for the object–color solid as a function of the spectral composition of daylights are small. Although the spectral composition of the illuminant in natural scenes also varies across the scene, and the application of the

color-difference formulas in these non-ideal conditions will produce only approximate results, Linhares *et al.* [11] considered it unlikely to influence the results critically. Masaoka *et al.* [12] proposed the number of discernible colors depends on the color appearance model, color space, and color difference limen used. Their results show that the number of discernible colors without a Von Kries color adaptation peaks at CCTs around 4000 K in CIELAB and CIE94 color spaces, and an increasing trend is found for CCTs in CIECAM02 and CAM02-UCS spaces in the range 2000 K–10,000 K, but they conclude the variations of this dependence were determined mainly by the chromatic adaptation transformation used.

Nascimento and Masuda [13] found a clear dependence of naturalness (how natural colors appear to observers) and preference (how pleasant the colors are) with illuminant CCT. Their results suggested that the most natural colors were produced under a CCT of 6040 K and the most preferred colors under a CCT of 4410 K. In addition, Nieves *et al.* [14] studied how color edges in natural scenes were influenced by natural illumination obtaining slight changes with CCT, but without differences between the postreceptoral responses to daylight variation. Nevertheless, the invariance in the spatial ratio of cone excitations arising from the color signal with changes in illumination may provide the basis of color constancy [15].

The aim of the present work was not only to analyze the influence of daylight changes in high-order statistics descriptors related with chromatic diversity (color volume and gamut, and number of discernible colors) but also to study their influence related to the regions of the images containing uniform areas or eye fixations in visual search. The dependence of the chromatic statistics descriptors on the salient regions was also considered. For that purpose, we used 350 color images, classified in seven semantic categories (forests and parks, fields, shores, mountains, beaches, rivers and waterfalls, and fruits and flowers), which were rendered under 108 natural illuminants with CCT from 2735 to 25,889 K.

2. METHODS

A. Images

We have used 350 RGB 400 × 400 pixels color images that were collected by the authors and also selected from the SUN Database [16]. The pictures were classified into seven semantic categories depending on their image content: Forests and Parks, Fields, Shores, Mountains, Beaches, Rivers and Waterfalls, and Fruits and Flowers. Every RGB image was normalized to the range (0, 1), and its CIE tristimulus values were found and simulated under a set of 108 daylights SPD characterized by their respective CCTs in the visible range [400–700] nm. The simulation was made using the Bradford chromatic adaptation algorithm:

$$\begin{pmatrix} X' \\ Y' \\ Z' \end{pmatrix} = \mathbf{M}_b^{-1} \begin{pmatrix} R'_W/R_W & 0 & 0 \\ 0 & G'_W/G_W & 0 \\ 0 & 0 & B'_W/B_W \end{pmatrix} \mathbf{M_b} \begin{pmatrix} X \\ Y \\ Z \end{pmatrix}, \tag{1}$$

where quantities R_w, G_w, B_w and R'_w, G'_w, B'_w were computed from the tristimulus values of the first and second illuminant using Judd color matching functions [17], and $\mathbf{M}_b$ is the Bradford matrix [18] defined as

$$\mathbf{M}_b = \begin{pmatrix} 0.8951 & 0.2664 & -0.1614 \\ -0.7502 & 1.7135 & 0.0367 \\ 0.0389 & -0.0685 & 1.0296 \end{pmatrix}. \tag{2}$$

Figure 1(a) shows examples of the same picture reproduced under three different illuminants (2735, 6478, and 25,889 K).

Daylights were measured in Granada, Spain, from sunrise to sunset under different atmospheric conditions, and cover a vast range of CCTs from 4800 K up to 30,000 K [7]. The simulated daylight SPDs were obtained with SBDART, a software tool to compute plane-parallel radiative transfer energy in clear and cloudy conditions within the Earth's atmosphere and at the surface [19] to cover CCTs below 4800 K.

Finally, the simulated pictures were transformed to CIELAB to benefit from the uniform color spaces to match the color properties of the environment with their visual representation [20]. Additional details about the validation and accuracy of the Bradford transform can be found in the Appendix section.

B. Data Analysis

The high-order statistical descriptors were the Patchiness Index (PI), the color gamut (CG), the color volume (CV), and the number of discernible colors (NdC) as described below. The NdC will be analyzed also in terms of the salient content in images.

1. Patchiness Index

The term "patchiness" was introduced by Yoonesi *et al.* [21] for describing the proportion of the image that contains uniform areas. An image with large uniform areas or with a lot of uniform areas will have a higher patchiness than an image with rare and small uniform regions. Patchiness is defined as the portion

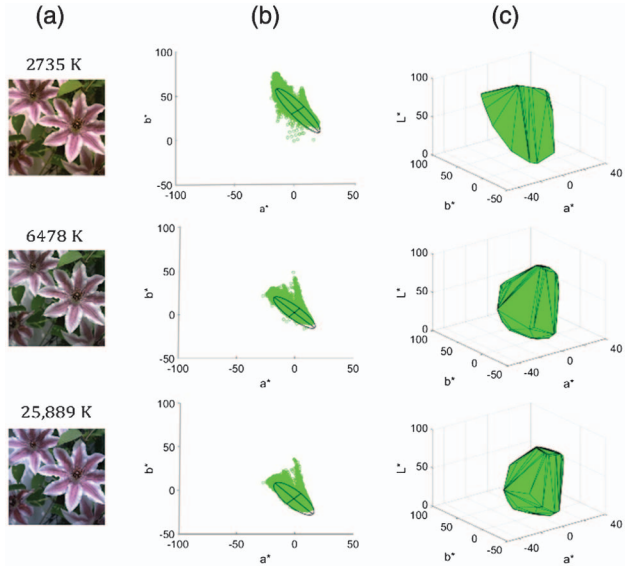

Fig. 1. (a) Three examples of the same picture simulated under different illuminants (2735, 6478, and 25,889 K). (b) Color gamut in the CIELAB (a*, b*) plane and corresponding best-fitting ellipses and (c) corresponding color volume of the pictures shown on the left.

of pixels falling within a ± threshold in the bandpass-filtered version of the image, averaged across multiple filter scales.

In this work the L*, a*, and b* planes of the images were filtered with isotropic log-Gabor filters defined in the Fourier domain as

$$\mathrm{LGF}(f,\theta)=\exp\left\{\left(-\log\left(\frac{R(f_i,\theta_j)}{F}\right)^2\right)\Big/\left(2\log\left(\frac{\sigma}{F}\right)^2\right)\right\}, \tag{3}$$

where f and θ are the polar coordinates of any point, R is the radius vector, F is the central spatial frequency, and σ is the spatial frequency bandwidth of the log-Gaussian function. These filters were not only used because they remove to zero the dc level of the image and represent quite well the cortical cells response, but also they are range independent; their responses are determined by the relations among pixels instead of the range of the input signal, and in that way, the calculation of the patchiness index for L*, a*, and b* channels of an image doesn't depend on the different signal levels of them. For that reason, when they are applied to noise-free images, the same value of patchiness is produced and uncorrelated Gaussian noise σ was added to each CIELAB plane set to 10% of the mean of the signal to avoid it [21].

Six spatial frequencies were used and the filtered images were then converted to binary images using an arbitrary fixed threshold set to ±0.07 from the mean. The use of a fixed threshold was based on its robustness to noise. The portion of pixels falling within the upper and lower threshold bounds was measured, and the patchiness index was calculated as the average of these values across the six filter scales.

2. Color Gamut and Color Volume

The color volume of each natural scene, defined as the palette of all available colors at all available intensities, was determined for all the illuminants. The color gamut was obtained by projecting the color volume into the plane (a*, b*) of CIELAB color space. The limits, shape, and orientation of the gamut for each image and each illuminant were characterized by the properties of an ellipse fitted to the data based on a least squares criterion. Area, axis ratio, and angular position were also estimated for each color gamut.

Figures 1(b) and 1(c) show examples of the color gamut with its best fitted ellipse and the color volume, respectively, of the same picture reproduced under illuminants 2735, 6478, and 25,889 K.

3. Number of Discernible Colors

The general principle behind the estimation of the number of discernible colors is to segment the color space in just noticeable subvolumes and to count the number of these containing the color representation of at least one pixel. The estimation of the number of discernible colors depends on the counting method (square-packing, ellipse-packing, or convex-hull) [12]. We used in this work the square-packing method that assumes a unit cube to be one discernible color in a Euclidean color space. The L*, a*, and b* values of each pixel of the picture were rounded to the nearest integer greater than or equal to the pixel value. In that way all the values falling inside the same cube are grouped in the upper corner of it.

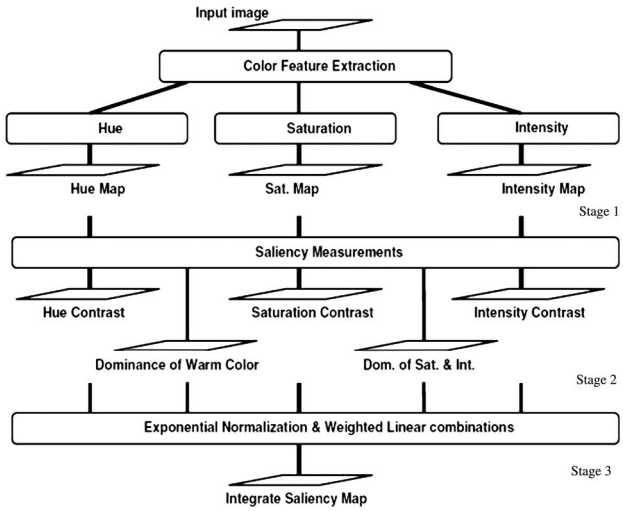

Fig. 2. Framework of Tian, Wan, and Yue [24] color saliency model.

4. Saliency Maps of Color Images

In addition to the high-order statistical descriptors, salience maps for all images were also computed. The saliency map is a biologically plausible model for bottom-up overt attention proposed by Koch and Ullman in 1985 [22]. In the review of the model by Itty *et al.* [23], the visual saliency maps are topographical codifications of fixation position in visual search over the entire scene based on different image features such as luminance, orientation, or color.

In the Tian, Wan, and Yue [24] color saliency model, which is used in this work, five saliency maps are obtained from every picture in the Hue-saturation-Intensity color space (HIS). These maps correspond to the following features: Contrast of hue, contrast of saturation, contrast of intensity, dominance of warm color, and dominance of brightness and saturation. Harel [25] implementation of the map normalization operator N(·) is applied to the features maps to globally promote them with a small number of strong peaks of activity (conspicuous locations) and suppress them with numerous comparable peak responses. The saliency map is a weighted linear combination of the five conspicuity maps normalized. Figure 2 summarizes the framework of the Tian, Wan, and Yue color saliency model we use.

3. RESULTS

A. Patchiness Index

The average values of PI for all CCTs and for all semantic categories were 0.940 ± 0.003, 0.93 ± 0.01, and 0.92 ± 0.01, for the L*, a*, and b*, respectively. As Table 1 shows, the order of CIELAB planes attending PI is L* > a* > b*, when the semantic categories of images are sorted by their PI values. Nevertheless, the values of the three planes are so similar that this order is not significant. Results show that when the semantic categories are arranged following an increasing or decreasing order of PI in one of the channels, there is no order in the other two channels.

Table 1. Patchiness Index (PI) in the Seven Semantic Categories Sorted by the Patchiness Index in L* Plane

	L*	a*	b*
Coasts	0.95	0.93	0.94
Fields	0.94	0.94	0.91
Flowers and fruits	0.94	0.91	0.90
Rivers and falls	0.94	0.92	0.94
Beaches	0.94	0.93	0.94
Forests and parks	0.94	0.92	0.89
Mountains	0.91	0.94	0.91
Natural images	0.94	0.92	0.92

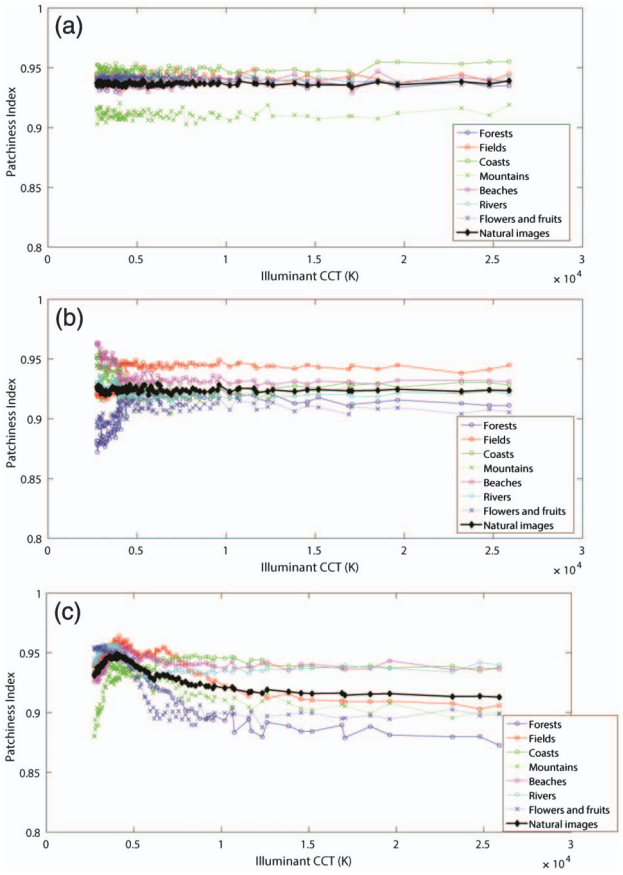

Fig. 3. Patchiness index for (a) L*, (b) a*, and (c) b*, respectively, categories as a function of illuminant CCTs.

Although the three components L*, a*, and b* do not show a meaningful variation of PI with CCT, all values are quite similar above a CCT of 7950 K [Figs. 3(a)–3(c)]. PI values for a* component, Fig. 3(b) shows almost constant variations around 0.92 and above a CCT of 4083 K. Figure 3(c) shows that the behaviors of all the categories in channel b* are similar to other descriptors presenting a local maximum in the range 2414–5611 K (except for Coasts category).

B. Color Gamut and Color Volume

Figure 4 shows the contour of color gamuts for the seven semantic categories of natural images simulated under two

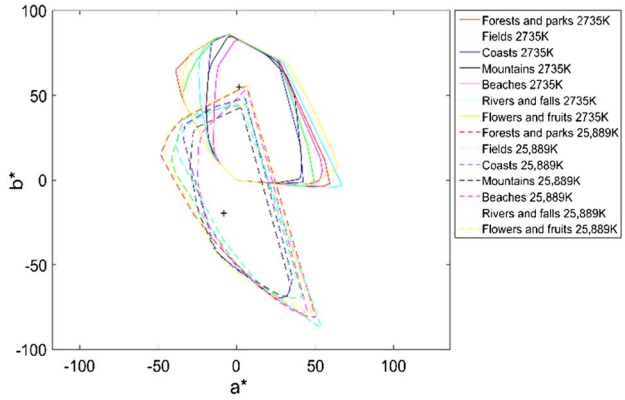

Fig. 4. Seven semantic categories color gamut contours under two different illuminants of CCTs 2735 K (solid lines) and 25,889 K (dashed lines). Chromatic coordinates of the corresponding whites are also shown for reference (crosses).

extreme illuminants (CCTs of 2735 and 25,889 K). At each CCT, all the categories have similar distribution of the color gamut ("Coasts," "Mountains," and "Beaches and fruits" have a smaller range in the a* channel). For both illuminants, the gamuts are elongated in the yellow-blue direction (except for "Forests and parks," "Flowers and fruits," and "Rivers and falls" at 2735 K) and the areas are bigger (except for "Mountains" and "Rivers and falls") at 25,889 K. Besides, at 2735 K the gamut centers are clearly shifted to red and yellow components (positive values in both axes) (8.59,38.35) but they are near centered in a* and shifted to blue components (negative value of b*) at 25,889 K (–1.69, –18.19).

The data obtained from the ellipses fitted to the colors of each scene and illuminants were averaged in the seven semantic categories. The distributions of the angles, axis ratios, and areas for different CCTs are represented separately for all the categories in Figs. 5(a)–5(c). Figure 5(a) shows the change of the angle of each ellipse along its positive axes. The values from 0° to 90° indicate an ellipse whose major axis is rotated to the right of coordinate b* and values from 90° to 180° indicate an ellipse rotated toward the left of coordinate b*. All the angles calculated for all the natural scenes under 108 illuminants are greater than 90°. And all the categories have local maxima in the range 3671–7406 K so for those temperatures the ellipses are more tilted to green. This effect does not mean that greens are more used than reds; rather, it means that the saturation balance favors greens over reds [26].

Figure 5(b) shows the changes with CCT of the axis ratios of the ellipses. The categories "Forests and parks" and "Flowers and fruits" present a distribution of colors more symmetrical than in the other categories (smaller values of axis ratio). The categories obtaining high ratios show a strong dependence with the illuminant CCT. All the categories show a local maximum in the range 6118–7209 K showing a more asymmetrical behavior towards the yellow-blue direction (b* component) at this CCT. For CCTs higher than 10,000 K, the ratio axis of all the categories presents the same dependence on illuminant CCTs, approaching a more symmetrical distribution of color with temperature.

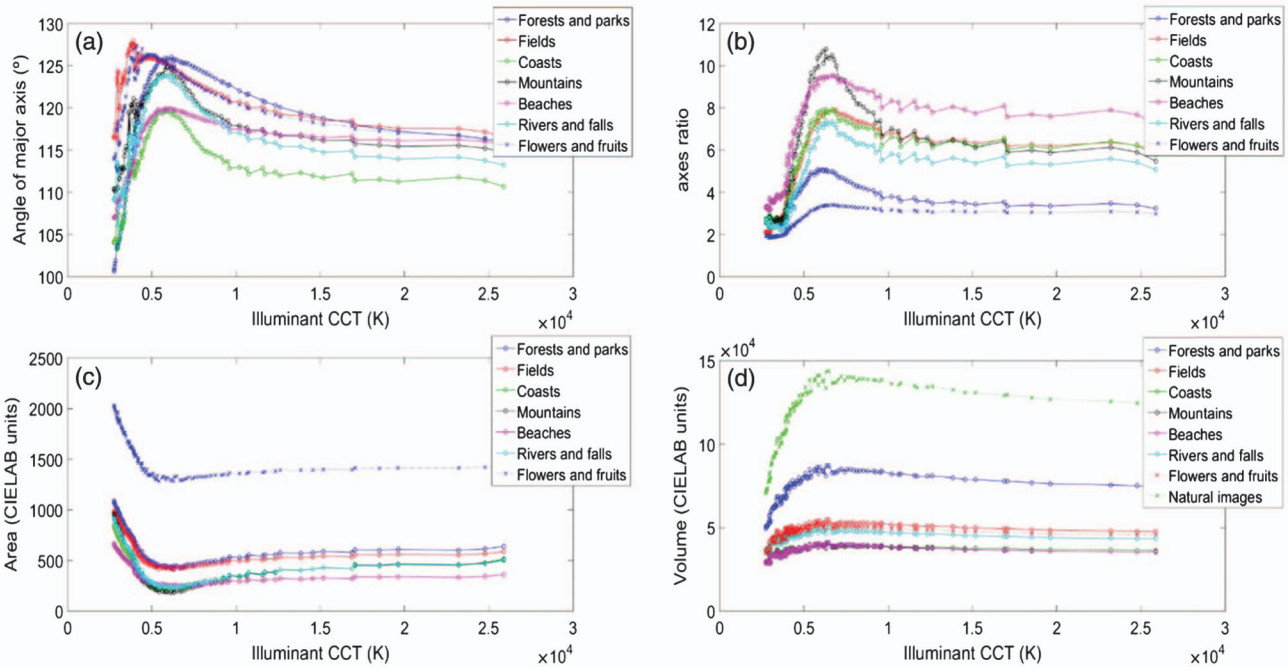

Fig. 5. (a) Best fitted ellipse angle, (b) axes ratio, (c) area, and (d) color volume obtained for all semantic image categories and CCT of the illuminants.

Figure 5(c) shows the changes with temperature of areas of the ellipses expressed in CIELAB units. The range of areas of the ellipses is 180–1085 for all the categories except for "Flowers and fruits," which is 1280–2735. Similar ellipse areas mean similar gamut limits but not necessarily similar color gamuts because the colors are not uniformly distributed within each ellipse. [26]. The area of all the categories show a similar response with illuminant CCT, having a local minimum in the range 5084–7209 K and being near constant for CCTs higher than 10,000 K.

Finally, Fig. 5(d) shows the changes with temperature of color volume in CIELAB units. All the categories present local minima at 3903 K and local maxima in the range of temperatures 6339–6478 K. Again for CCTs higher than 12,000 K, the color volume is nearly constant. The categories obtaining high volumes show a strong dependence on illuminant CCT compared to the other ones. The local maxima in color volume at the same daylight CCTs that color gamut have local minima are due to the L* component.

C. Number of Discernible Colors

Figure 6 shows the process followed to mask the original images with their saliency maps. The original CIELAB images are first converted to HSI images and the integrated saliency map is calculated. Next the salient objects are extracted from their background segmenting the integrated saliency map, and a thresholding method [27] with threshold the average of the integrated saliency map is used. A region of interest (ROI) map is applied to the segmented saliency map to remove noise [28], and finally HSI images are masked with ROI maps and converted back to CIELAB image format.

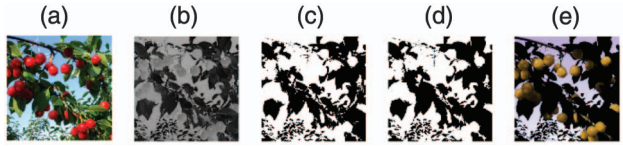

Fig. 6. Masking original images with their integrated saliency maps process: (a) original image, (b) integrated saliency map, (c) integrated saliency map segmented, (d) ROI map, and (e) masked image with ROI map.

Figure 7(a) shows the changes in CCT of the number of discernible colors using the square-packing method of the seven semantic categories and the average value for the set of all the natural images used. Due to the method used, the distribution we get is similar to the distribution of the color volume of each category. All categories present a quick increase in their color volumes below the local maxima around 6339–6478 K. The number of discernible colors is fairly constant for temperatures higher than 9600 K.

Figure 7(b) shows the changes in temperature of the number of discernible colors of the masked images. Results suggest also an increasing trend in the number of discernible colors found below the local maxima at 6339 K–6478 K (except "Forests and parks," "Fields," and "Flowers and fruits," for which maxima are at higher temperatures). The number of discernible colors of the salient regions is fairly constant for CCTs higher than 14,000 K.

In Table 2, the range of the number of discernible colors is shown for each category and for original images and salient regions; the percentage of reduction of the average number of

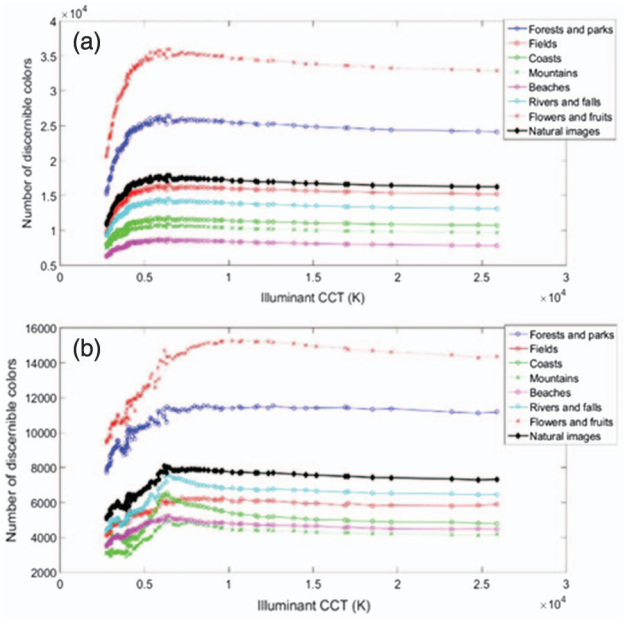

Fig. 7. Number of discernible colors as a function of the illuminant CCTs for (a) the original images, and (b) the masked images with their saliency maps.

discernible colors between the salient regions and the original images is also computed. When the salient regions of the original images are considered instead of them, a reduction of number of discernible colors between 44% and 63% is obtained. Obviously the number of discernible colors in the salient regions should be below the corresponding number when the whole image is considered (as the salient region will contain less number of pixels). To check the proportion of this reduction corresponding to a salient region, every computed ROI map was flipped horizontally and vertically and rotated 180°. The images were subsequently masked again with the transformed maps and the number of discernible colors were computed for those new areas. The results show that the reduction in the number of discernible colors for the salient regions is always 10%–17% above the number obtained when salient regions are not considered in the computation, i.e., using the rotated and flipped mask, even considering that the number of pixels in both computations was kept constant; this result is general for all semantic categories except beaches where the number is almost constant.

Table 2. Range of Number of Discernible Colors of the Original Images, Their Salient Regions, and the Average Percentage of Reduction between Them

	Range of NDC for Original Images	Range of NDC for Salient Regions	Average Percentage of Reduction (%)
Fields	9500–16,510	4096–6251	63
Mountains	7510–10,890	2875–5095	61
Flowers & fruits	20,530–35,980	9402–15,260	60
Forests & parks	26,360–15,210	7716–11,530	56
Coasts	7924–11,820	3458–6536	56
Rivers & falls	9254–14,460	4346–7582	55
Beaches	6291–8750	3495–5224	44
Natural images	10,890–17,820	5083–8056	58

4. DISCUSSION AND CONCLUSIONS

The aim of this work was not only to analyze the influence of daylight CCTs changes in different high-order chromatic descriptors (color volume, color gamut, and number of discernible colors) but also to study its influence related to the regions of the images containing uniform areas (as described by patchiness values) and the constraint imposed by saliency maps simulating potential observers' eye fixations during a visual search task.

Based on the definition of patchiness, as a descriptor of the uniform areas in a scene, the chromatic channels should have greater patchiness values than the luminance component; in addition, changes in chromatic a* and b* components represent more faithfully the layout of object surfaces than the luminance component that usually supports shadows and shadings. Patchiness results in Yoonesi *et al.* [21] support the idea that spatial resolution of postreceptoral channels has evolved to reflect patchiness. The order of CIELAB planes attending Patchiness Index is $L^* < b^* < a^*$, which is the same order of postreceptoral channels to sensitivity of shadows and shading [29–31], and spatial resolution [32,33]. Nevertheless, the differences found for the three color channels across different daylight CCTs are not relevant to clearly establish a conclusion about this dependency, particularly if noise is not described and computed. Although the images' data set was classified in seven semantic categories, all the statistics descriptors analyzed have similar behavior with CCT.

The analysis of the best fitting ellipses describing the color gamut of all natural scenes reveals shapes that are elongated in the b* direction [20,34,35] and tilted to negative values of a* (i.e., greenish component) [26]. The shift to negative values of both chromatic axes of the gamut centers with CCTs justifies why images look more bluish when CCT is high.

Pointer and Attridge [36] estimated the number of discernible colors at about 2.28 million using the square-packing method under illuminant D65 in the CIELAB color space and idealized object–color solid. Nevertheless, we got a number of discernible colors between 4705 and 25,726 using daylight and the same color space and counting method. Linhares *et al.* [11] estimated the number of discernible colors at about 2.7×10^5 considering the three components of CIEDE2000 color space, suggesting the reduction of number of discernible colors of the natural images from the total estimated is due to the natural spectral reflectances that are different from the idealized ones.

But color diversity, which is introduced as the number of discernible colors, could depend on other visual cues. Amano *et al.* [37] found that 57%–60% of the variance in observers' detection performance over scenes could be explained by local color properties in the CIECAM02 color space, a level

closely similar to that explained by the distribution of observers' fixations. But the ability of an observer to perceptually identify distinct surfaces in natural scenes by virtue of their color depends not only on the relative frequency of surface colors but also on the probabilistic nature of observer judgments. When information-theoretic methods (based on the mutual information descriptor) are used instead of a deterministic approach to take into account both differing surface-color frequencies and observer response uncertainty in the number of distinct surface colors, estimation was about 7.3×10^3 in the CIECAM02 color space [38], more than an order of magnitude lower than the number reported by Linhares *et al.* [11]. When only salient regions of the images were considered an average reduction of the number of discernible colors of 58% was obtained in our work, being similar to the number of 5.2×10^3 obtained by Marin-Franch and Foster [38].

Because the number of colors discernible by the HVS is unlimited and cannot be associated with a single illuminant, color constancy can be also understood as an adaptive mechanism for reducing the diversity of distinguishable colors without common perceptual correspondence with multiple illuminations [10]. On the one hand the significant reduction of discernible colors in the salient regions could support that idea, but on the other it is a question of further studies to clarify the first and parallel stage (top-down process) of the visual attention mechanisms [22].

Besides these results, most of the computed statistical descriptors hardly depended on illuminant CCTs for temperatures higher than 10,000 K and showed local extremes in the range 2950 K–6300 K. This range could be related with the values of the average CCT illuminant established by Masuda and Nascimento [39] for the most natural and the most preferred colors (6040 K and 4410 K, respectively), suggesting that effectively other color vision-related topics could be optimized for those illuminations.

APPENDIX A

In this section, validation of the Bradford Chromatic Transform (BCT) in scene reproduction under different illuminants is provided.

The BCT is a chromatic adaptation-based transform that models illumination change providing specifically a mapping of tristimulus values XYZs under a reference source to XYZs for a target light. We have performed an evaluation of the BCT simulating a set of hyperspectral scenes under three illuminants from our daylight set (CCTs of 2735, 6478, and 25,889 K). These scenes will be considered as the reference scenes to be compared with the prediction derived from the BCT. A source daylight illumination of 6478 K is used as a reference in the BCT Eqs. (1) and (2). Hyperspectral scenes were obtained from the Nascimento's set, which is available online at http://online.uminho.pt/pessoas/smcn/hsi_2002/hsi_2002.html; urban and/or artificial scenes were avoided for this computation.

The average CIELAB color difference for all scenes used was 12.5 (4.5 standard deviation) for 2735 K and 14.5 (3.1 standard deviation) for 25,889 K. Figure 8 below shows examples obtained for two images under 2735 and 25,889 K illuminations, showing the BCT image in the left column, and the histogram of CIELAB color differences between the two illuminant conditions in the right column.

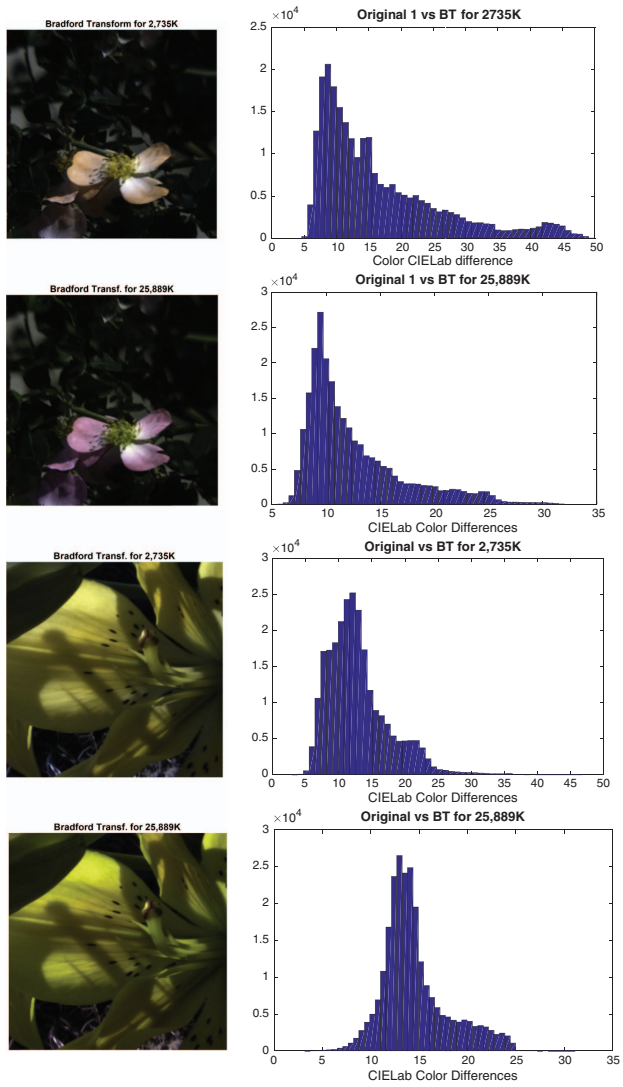

Fig. 8. Bradford chromatic transformed (BCT) images (in the left column) and histogram of CIELAB color differences (in the right column) for two scenes under illuminants of 2735 and 25,889 K CCTs.

Funding. Ministerio de Economía y Competitividad (MINECO) (DPI2015-64571-R).

REFERENCES

1. W. S. Geisler, "Visual perception and the statistical properties of natural scenes," Annu. Rev. Psychol. **59**, 167–192 (2008).
2. E. P. Simoncelli and B. A. Olshausen, "Natural images statistics and neural representation," Annu. Rev. Neurosci. **24**, 1193–1216 (2001).
3. G. Buchsbaum and A. Gottschalk, "Trichromacy, opponent colours coding and optimum colour information transmission in the retina," Proc. R. Soc. London B **220**, 89–113 (1983).
4. D. L. Ruderman, T. W. Cronin, and C. C. Chiao, "Statistics of cone responses to natural images: implications for visual coding," J. Opt. Soc. Am. A **15**, 2036–2045 (1998).

5. T. Wachtler, E. Doi, T. Lee, and T. J. Sejnowski, "Cone selectivity derived from the responses of the retinal cone mosaic to natural scenes," J. Vis. **7**(8), 6 (2007).
6. T. Wachtler, T.-W. Lee, and T. Sejnowski, "Chromatic structure of natural scenes," J. Opt. Soc. Am. A **18**, 65–77 (2001).
7. J. Hernández-Andrés, J. Romero, J. L. Nieves, and R. L. Lee, Jr., "Color and spectral analysis of daylight in southern Europe," J. Opt. Soc. Am. A **18**, 1325–1335 (2001).
8. C. C. Chiao, T. W. Cronin, and D. Osorio, "Color signals in natural scenes: characteristics of reflectance spectra and effects of natural illuminants," J. Opt. Soc. Am. A **17**, 218–224 (2000).
9. D. H. Foster, "Color constancy," Vis. Res. **51**, 674–700 (2011).
10. F. Martinez-Verdu, E. Perales, E. Chorro, D. de Fez, V. Viqueira, and E. Gilabert, "Computation and visualization of the MacAdam limits for any lightness, hue angle, and light source," J. Opt. Soc. Am. A **24**, 1501–1515 (2007).
11. J. M. M. Linhares, P. D. Pinto, and S. M. C. Nascimento, "The number of discernible colors in natural scenes," J. Opt. Soc. Am. A **25**, 2918–2923 (2008).
12. K. Masaoka, R. S. Berns, M. D. Fairchild, and F. M. Abed, "Number of discernible object colors is a conundrum," J. Opt. Soc. Am. A **30**, 264–277 (2013).
13. S. M. C. Nascimento and O. Masuda, "Psychophysical optimization of lighting spectra for naturalness, preference, and chromatic diversity," J. Opt. Soc. Am. A **29**, A144–A150 (2012).
14. J. L. Nieves, S. M. C. Nascimento, and J. Romero, "Contrast edge colors under different natural illuminations," J. Opt. Soc. Am. A **29**, A240–A246 (2012).
15. S. M. C. Nascimento, K. Amano, and D. H. Foster, "Spatial distributions of local illumination color in natural scenes," Vis. Res. **120**, 39–44 (2016).
16. J. Xiao, J. Hays, K. Ehinger, A. Oliva, and A. Torralba, "SUN database: large-scale scene recognition from Abbey to Zoo," in *IEEE Conference on Computer Vision and Pattern Recognition* (2010).
17. D. B. Judd, "Report of U.S. secretariat committee on colorimetry and artificial daylight," in *Proceedings of the 12th Session of the CIE*, Stockholm, Sweden (Bureau Central de la CIE, 1951), Vol. **1**, pp. 11.
18. S. Süsstrunk, J. Holm, and G. D. Finlayson, "Chromatic adaptation performance of different RGB sensors," in *Proceedings of IS&T/SPIE Electronic Imaging: Color Imaging* (2001), Vol. **4300**, pp. 172–183.
19. P. Ricchiazzi, S. Yang, C. Gautier, and D. Sowle, "SBDART: a research and teaching software tool for plane-parallel radiative transfer in the earth's atmosphere," Bull. Am. Meteorol. Soc. **79**, 2101–2114 (1998).
20. K. C. McDermott and M. A. Webster, "Uniform color spaces and natural image statistics," J. Opt. Soc. Am. A **29**, 182–187 (2012).
21. A. Yoonessi, F. A. A. Kingdom, and S. Alqawlaq, "Is color patchy?" J. Opt. Soc. Am. A **25**, 1330–1338 (2008).
22. C. Koch and S. Ullman, "Shifts in selective visual attention: towards the underlying neural circuitry," Human Neurobiology **4**, 219–227 (1985).
23. L. Itti, C. Koch, and E. Niebur, "A model of saliency-based visual attention for rapid scene analysis," IEEE Trans. Pattern Anal. Mach. Intell. **20**, 1254–1259 (1998).
24. M. Tian, S. Wan, L. Yue, and A. Color, "Saliency model for salient objects detection in natural scenes," in *Conference paper MMM 2010*, Chongqing, China (2010), pp. 6–8.
25. J. Harel, "A Saliency Implementation in MATLAB," (2013), http://www.klab.caltech.edu/~harel/share/gbvs.php.
26. C. Montagner, J. M. M. Linhares, M. Vilarigues, and S. M. C. Nascimento, "Statistics of colors in paintings and natural scenes," J. Opt. Soc. Am. A **33**, A170–A177 (2016).
27. C. A. Glasbey and G. W. Horgan, *Image Analysis for the Biological Sciences* (Wiley, 1995).
28. R. Bharath, L. Z. J. Nicholas, and X. Cheng, "Scalable scene understanding using saliency-guided object localization," in *10th IEEE International Conference on Control and Automation (ICCA)* (2013).
29. C. A. Parraga, G. Brelstaff, T. Troscianko, and I. R. Moorehead, "Color and luminance information in natural scenes," J. Opt. Soc. Am. A **15**, 563–569 (1998).
30. C. A. Párraga, T. Troscianko, and D. J. Tolhurst, "Spatiochromatic properties of natural images and human vision," Curr. Biol. **12**, 483–487 (2002).
31. F. A. Kingdom, C. Beauce, and L. Hunter, "Colour vision brings clarity to shadows," J. Vis. **3**, 637 (2003).
32. K. T. Mullen, "The contrast sensitivity of human colour vision to red–green and blue–yellow chromatic gratings," J. Physiol. **359**, 381–400 (1985).
33. G. J. C. Van Der Horst and M. A. Bouman, "Spatiotemporal chromaticity discrimination," J. Opt. Soc. Am. **59**, 1482–1488 (1969).
34. M. A. Webster and J. D. Mollon, "Adaptation and the color statistics of natural images," Vis. Res. **37**, 3283–3298 (1997).
35. S. M. C. Nascimento, F. P. Ferreira, and D. H. Foster, "Statistics of spatial cone-excitation ratios in natural scenes," J. Opt. Soc. Am. A **19**, 1484–1490 (2002).
36. M. R. Pointer and G. G. Attridge, "The number of discernible colours," Color Res. Appl. **23**, 52–54 (1998).
37. K. Amano, D. H. Foster, M. S. Mould, and J. P. Oakley, "Visual search in natural scenes explained by local color properties," J. Opt. Soc. Am. A **29**, A194–A199 (2012).
38. I. Marin-Franch and D. H. Foster, "Number of perceptually distinct surface colors in natural scenes," J. Vis. **10**(9), 9 (2010).
39. O. Masuda and S. M. C. Nascimento, "Best lighting for naturalness and preference," J. Vis. **13**(7), 4 (2013).